Available online at www.sciencedirect.com
ScienceDirect
Ceramics International 37 (2011) 2569–2574
CERAMICS INTERNATIONAL
www.elsevier.com/locate/ceramint

Fabrication and characterization of a Ni-YSZ anode support using high-frequency induction heated sintering (HFIHS)

Jong-Yeol Yoo [a], In-Jin Shon [a,b], Byung-Hyun Choi [c], Ki-Tae Lee [a,b,*]

[a] Department of Hydrogen Fuel Cells Engineering, Specialized Graduate School, Chonbuk National University, Jeonbuk 560-756, Republic of Korea
[b] Division of Advanced Materials Engineering, Chonbuk National University, Jeonbuk 560-756, Republic of Korea
[c] Optic and Electronic Ceramics Division, Korea Institute of Ceramic Engineering and Technology, Seoul 153-801, Republic of Korea

Received 17 January 2011; received in revised form 23 March 2011; accepted 1 April 2011
Available online 8 April 2011

Abstract

Ni-YSZ cermet anode supports solid oxide fuel cells (SOFCs) were fabricated by high-frequency induction heated sintering (HFIHS) under 60 MPa pressure with powders synthesized by the glycine nitrate process (GNP) as well as mechanically mixed commercial powders. The HFIHS method created a uniformly porous microstructure without abnormal grain growth compared to the conventional sintering method. Samples sintered by HFIHS show higher strength and electrical conductivity than conventionally sintered samples, even though they have similar porosity.

Keywords: Solid oxide fuel cell; Anode support; Rapid sintering; Microstructure

1. Introduction

Anode-supported solid oxide fuel cells (SOFCs) have been investigated to obtain high performance in SOFCs [1–3]. Electrolytes in SOFCs should be as thin as possible to reduce ohmic loss. Therefore, use of the anode-supported type SOFC is a good way to decrease operating temperatures and improve performance, because these can reduce the thickness of electrolytes below 20 μm. Anode supports for SOFCs should have appropriate mechanical strength, good microstructure with sufficient porosity to supply fuel gases and emit reaction products, and high thermal shock resistance [4–6]. The triple-phase boundary (TPB) where the electrolyte, gas, and electrically connected electrode meet is a particularly important part of the anode, because the hydrogen oxidation reaction can only occur at the TPB [7]. Because the extension of TPB can enhance performance, microstructure and connectivity must be controlled to extend the TPB.

High-frequency induction heated sintering (HFIHS) creates fully dense sintered bodies and controls microstructure during the sintering process [8–10]. Although rapid grain growth occurs during conventional sintering processes, such as solid state reaction, the HFIHS method suppresses abnormal grain growth due to its relatively short sintering time (5 min). We used the HFIHS method to control the microstructure of porous anode supports without abnormal grain growth during sintering, which can increase the size of the TPB and result in performance improvements. The anode sintering process was conducted with different powder particle sizes under various pressures.

2. Experimental procedure

Two different types of NiO-YSZ powders (Ni:YSZ = 60:40 vol.%) were prepared. One was the FP sample that mixed with commercial NiO (F.P., Japan) and YSZ (Tosoh, Japan) by ball milling for 12 h. The other was the GP sample that was a very fine powder co-synthesized by the glycine nitrate process (GNP). The powder prepared by GNP was calcined at 600 °C for 2 h and then milled with zirconia balls for 24 h [11,12].

NiO-YSZ pellets were sintered by HFIHS within 3 min from the prepared NiO-YSZ powder in a graphite die (outside diameter, 45 mm; inside diameter, 20 mm; height, 40 mm) under uniaxial pressures of 40, 60, and 80 MPa. The process

* Corresponding author at: Division of Advanced Materials Engineering, Chonbuk National University, Jeonbuk 560-756, Republic of Korea.
Tel.: +82 63 270 2290; fax: +82 63 270 2386.
E-mail address: ktlee71@jbnu.ac.kr (K.-T. Lee).

0272-8842/$36.00
doi:10.1016/j.ceramint.2011.04.002

was carried out under a 133 Pa vacuum. The HFIHS apparatus includes a 15 kW power supply with a 50 kHz frequency and a 50 kN uniaxial press. For comparison, another NiO-YSZ pellet was sintered by the conventional solid state reaction method at 1400 °C for 4 h.

Phase analysis and crystal size were determined by X-ray diffraction (XRD, MAX-111A, Rigaku Corporation, Japan). Morphology and grain size of samples were observed by scanning electron microscopy (SEM, S-4800, Hitachi, Japan). Ni in the reduced samples was removed in HCl solution. The Archimedes method was used to determine apparent porosity of the reduced samples, and pore size distribution was measured with a mercury porosimeter (UPA-150, Microtrac, USA). Flexural strength was measured by 3-pont bend test with universal testing machine (US/5884, Instron, USA). Samples with 20 mm × 5 mm × 2 mm bar shape were cut from the sintered body. The test speed was 0.2 mm/min using a 3-point support in a universal test machine with a span of 20 mm at room temperature [13]. Electrical conductivity was measured in a hydrogen atmosphere using the DC 4-probe method in the range of 400–800 °C, at 100 °C increments.

3. Results and discussion

XRD patterns of the NiO-YSZ cermet powder co-synthesized by GNP and calcined at 600 °C for 2 h are shown in Fig. 1. All peaks demonstrate that NiO and YSZ are well co-synthesized by GNP without any impurity. Crystallite sizes calculated by Stokes and Wilson's formula [14] from XRD data are reported in Table 1. The crystallite sizes of NiO and YSZ co-synthesized by GNP were 21 and 11 nm, respectively. However, NiO and YSZ in the FP powder have much larger crystallite size compared with those in the GP powder. This is also confirmed by the morphology of the prepared powders, shown in Fig. 2. While the FP powder has large NiO particles, the GP powder is very fine with uniform distribution of NiO and YSZ.

Table 1
Crystallite size of starting powder.

Sample	Component	Crystallite size (nm)
GP	NiO	21
	YSZ	11
FP	NiO (F.P.)	200
	YSZ (Tosoh)	63

The HFIHS sintering process consists of several steps. The first step is introducing uniaxial pressure and evacuation, the second is inducing current, and the final step is densification. Current was induced until variations of shrinkage under pressure with heating time for NiO-YSZ ceased. Fig. 3 shows sintering behaviors of all GP and FP samples. An initial increase in shrinkage displacement within 10 s is due to abrupt temperature increase with current induction and the applied pressure; shrinkage rate then increases gradually with temperature, due to consolidation. In all samples, contraction increases with increased pressure. The GP samples, however, showed faster contraction kinetics and lower sintering temperatures than the FP samples because of the smaller particle size of the GP powder. More importantly, all sintering processes finish within 3 min and below 1200 °C, which can suppress grain growth.

In general, pores in Ni-YSZ cermet anodes without pore formers are derived from two sources. One is the process of

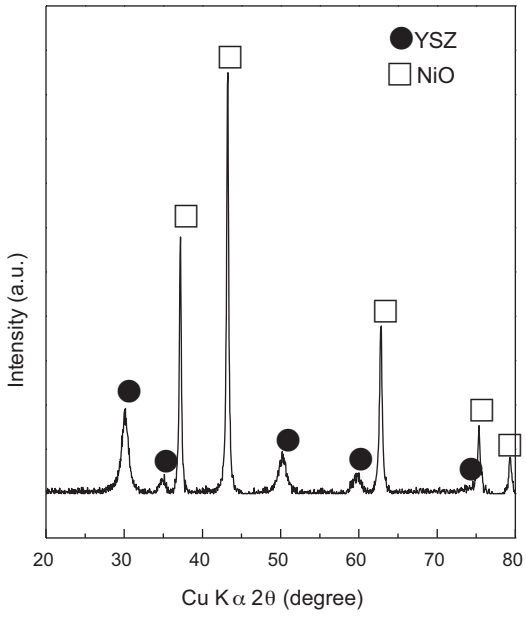

Fig. 1. X-ray diffraction pattern of the GP powder co-synthesized by GNP.

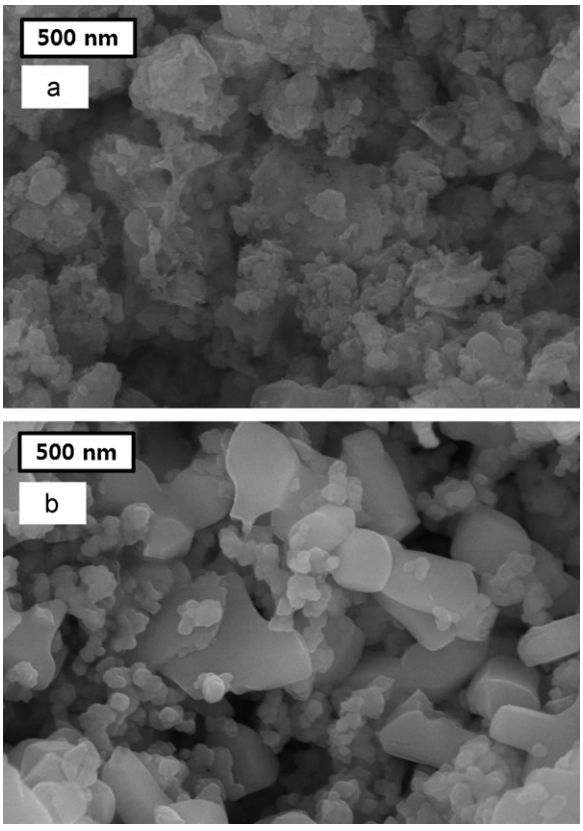

Fig. 2. SEM micrograph of starting powders; (a) GP powder and (b) FP powder.

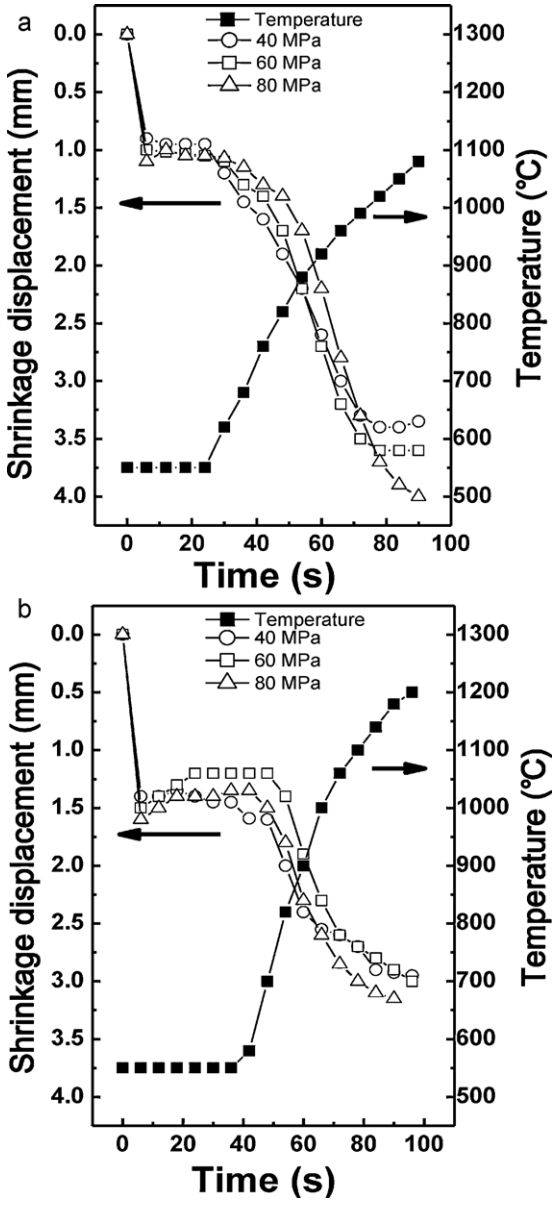

Fig. 3. Variation of temperature and shrinkage displacement of NiO-YSZ support with heating time during HFIHS; (a) GP sample and (b) FP sample.

incomplete sintering and the other is the reduction of NiO. Therefore, initial particle size, connectivity, and grain growth of NiO are critical to control the porous microstructure. Fig. 4 shows images of the surfaces of specimens successfully sintered by HFIHS with GP and FP powders under a pressure of 60 MPa. The grains of both powders remain similar to those of the raw powders, without abnormal grain growth during HFIHS. It is clear that fine pores are uniformly distributed, and the network structures of YSZ are well built up with good connectivity. Meanwhile, there is no appreciable difference in microstructure at various pressures, as shown in Fig. 5. The calculated apparent porosities of the reduced samples sintered by HFIHS with GP and FP powders are listed in Table 2. The samples show similar values of apparent porosity across the range of applied pressures during sintering. This result corresponds to the microstructures shown in Fig. 5. However, the FP samples have apparent porosities around 28%, and the GP samples have about 24%. This might be a result of capillary force from the very fine pores of the GP samples. The capillary force would interfere with water soaking into samples, and might cause the difference in porosity.

Fig. 6 shows the microstructures of samples sintered by the conventional solid state reaction method. Compared with the sample sintered by HFIHS shown in Fig. 4, there are relatively large grains due to the high sintering temperature of 1400 °C and the 4 h soaking time. In particular, there are very large Ni grains resulting from abnormal grain growth of NiO, which is evidenced by large pores in the Ni-removed sample.

Porosity and average pore size of the samples sintered by HFIHS and the conventional method (CS) are listed in Table 3. Porosity measured with the mercury porosimeter is 3–9% higher than apparent porosity. As mentioned earlier, this difference is a result of capillary force. The large pore sizes in the samples sintered by the conventional method are evidence for NiO grain growth during conventional sintering. On the other hand, significant grain growth did not occur in the samples fabricated by HFIHS, because of the fast sintering time and low sintering temperature. Interestingly, despite similar porosity, the samples fabricated by HFIHS have much smaller pore sizes than those fabricated by conventional sintering. This means that HFIHS method can create a porous microstructure that maintains the initial powder morphology. Consequently, one can easily control the porous microstructure by modifying starting powders and pore formers.

The flexural strengths of the reduced samples are presented in Fig. 7. The samples sintered by HFIHS show higher strength than the conventionally sintered samples, even though they have similar porosity. Because pores act as the origins of fractures, rupture strength decreases with increasing pore size and porosity. Flexural strength correlates well to pore size distribution results for the reduced samples, as shown in Table 3. The GP samples have higher strengths than the FP samples.

Table 2
Apparent porosity of reduced samples measured by Archimedes method.

Sample	Porosity (%)				
	HFIHS				CS
	40 MPa	60 MPa	80 MPa	60 MPa holding for 2 min	1400 °C, 4 h
GP	23	24	24	23	24
FP	27	28	28	28	25

Table 3
Porosity and average pore size of the reduced samples.

Sample	Porosity (%)		Average pore size (nm)	
	By Archimedes method	By mercury prosimeter	Reduced	Ni-removed
HFIHS GP	24	33	93	100
CS GP	24	30	178	489
HFIHS FP	28	31	232	370
CS FP	25	32	321	642

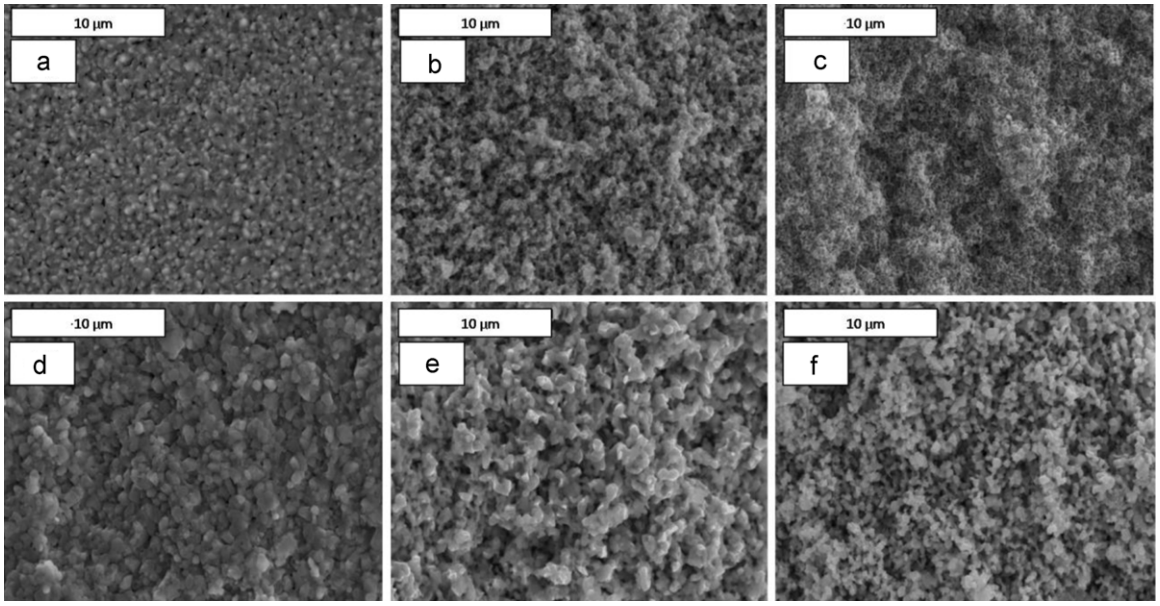

Fig. 4. SEM micrographs of the specimens sintered by HFIHS with (a–c) GP powder and (d–f) FP powder under a pressure of 60 MPa. (a) and (d) sintered body; (b) and (e) reduced body; (c) and (f) Ni-removed body.

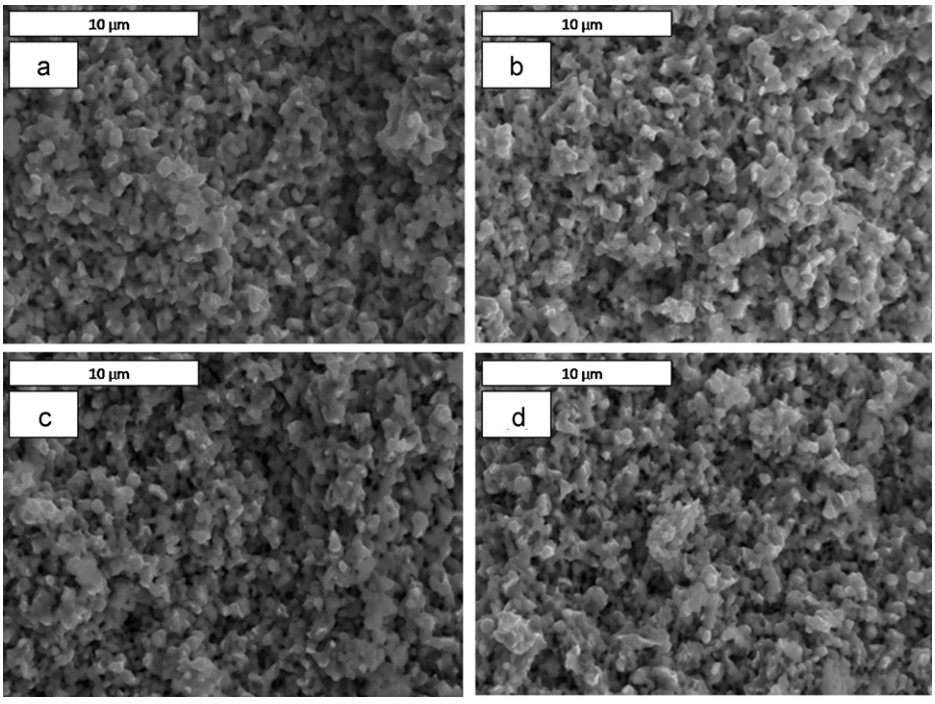

Fig. 5. SEM micrographs of NiO-YSZ support fabricated by HFIHS with FP powder holding for 2 min under (a) 80 MPa, (b) 60 MPa, (c) 40 MPa, and (d) 60 MPa.

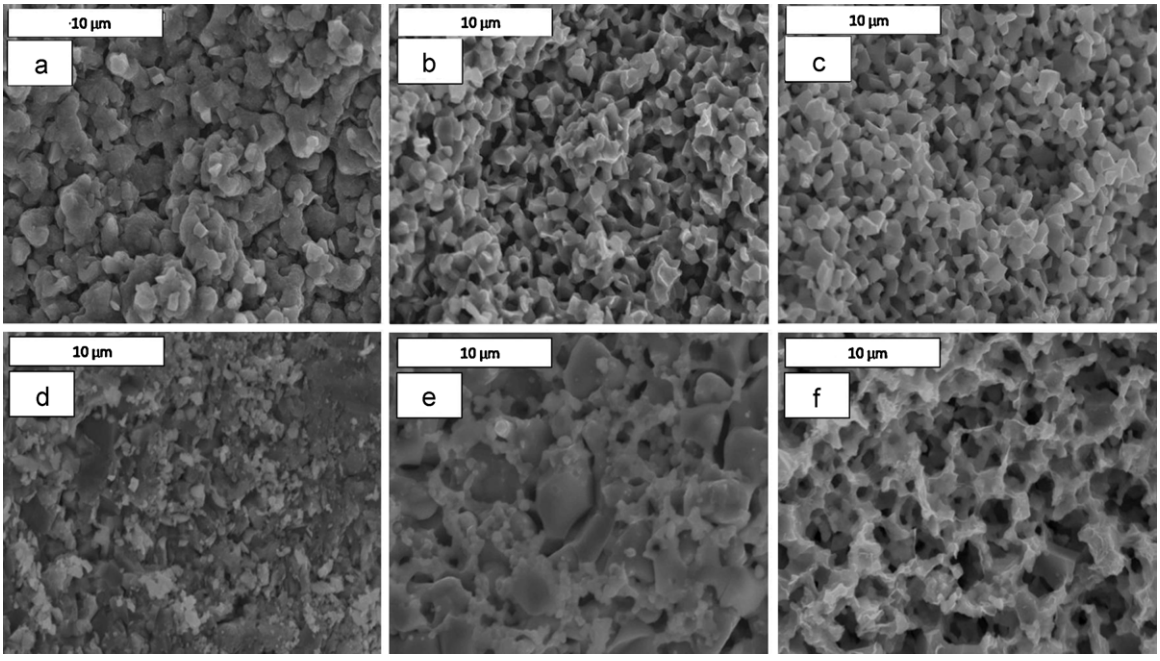

Fig. 6. SEM micrographs of samples sintered by conventional method with (a–c) GP powder and (d–f) FP powder. (a) and (d) sintered body; (b) and (e) reduced body; (c) and (f) Ni-removed body.

This might be due to the irregular particle size distribution of the initial FP powder.

The electrical conductivities of Ni-YSZ cermet anode supports measured in a hydrogen atmosphere are shown in Fig. 8. Electrical conductivity of a Ni-YSZ cermet is strongly dependent on its Ni content. The percolation threshold for metallic conduction is about 30 vol.% Ni [15]. Because all samples contain 60 vol.% Ni, the conductivity of the cermets decreases with increasing temperature. The electrical conductivities of the HFIHS samples are higher than those of the CS samples, and the FP samples have higher conductivity than the GP samples. The electrical conductivity of the cermet also depends on its microstructure. Ni particle-to-particle contact is important to obtain higher conductivity for the cermet. At the same Ni content, the HFIHS samples show more uniform contact between Ni particles than the CS samples, as shown in Figs. 4 and 6, resulting in higher electrical conductivity. Meanwhile, bigger Ni grains in the FP samples could lead to area contact and coverage between Ni particles. This may result in higher electrical conductivity for the FP samples than the GP samples.

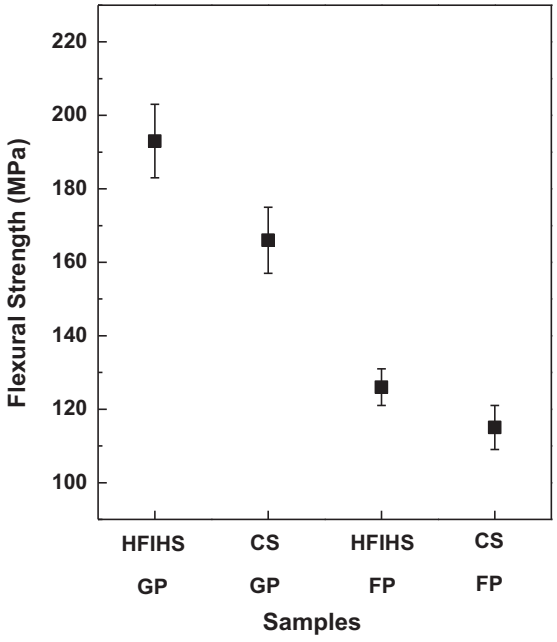

Fig. 7. Flexural strengths of the reduced samples.

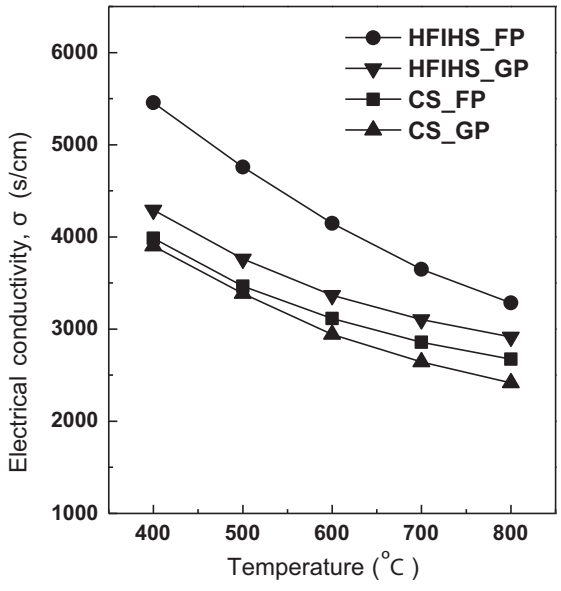

Fig. 8. Variations in electrical conductivity of the Ni-YSZ cermet measured in a hydrogen atmosphere.

4. Conclusions

Fine NiO-YSZ powder was co-synthesized by GNP. The crystallite sizes of NiO and YSZ were 21 and 11 nm, respectively. Porous anode supports for SOFCs were successfully manufactured by HFIHS. In HFIHS, sintering time and temperature are dramatically reduced compared to conventional sintering methods. The microstructure was not affected by pressure during the HFIHS sintering process. At similar porosities, the samples sintered by HFIHS show higher strength and electrical conductivity than conventionally sintered samples due to uniform pore and grain distribution and better Ni particle-to-particle contact. Consequently, HFIHS controls the porous microstructure in Ni-YSZ cermet anode supports without grain growth. A tailor-made process for increasing TPB is possible, and samples with appropriate character could be obtained by changing the characteristics of the starting powders, resulting in performance improvements.

Acknowledgement

This research was supported by a grant from the Fundamental R&D Program for Core Technology of Materials funded by the Ministry of Knowledge Economy, Republic of Korea.

References

[1] L. Zhang, S.P. Jiang, W. Wang, Y. Zhang, NiO/YSZ, anode-supported, thin-electrolyte solid oxide fuel cells fabricated by gel casting, J. Power Sources 170 (2007) 56–60.
[2] Y.H. Du, N.M. Sammes, Fabrication and properties of anode-supported tubular solid oxide fuel cells, J. Power Sources 136 (2004) 66–71.
[3] Y.H. Zhang, X. Huang, Z. Lu, Z. Liu, X. Ge, J. Xu, X. Xin, X. Sha, W. Su, Ni–$Sm_{0.2}Ce_{0.8}O_{1.9}$ anode-supported YSZ electrolyte film and its application in solid oxide fuel cells, J. Alloys Compd. 428 (2007) 302–306.
[4] S.T. Aruna, M. Muthuraman, K.C. Patil, Synthesis and properties of Ni-YSZ cermet: anode material for solid oxide fuel cells, Solid State Ionics 111 (1998) 45–51.
[5] U. Anselmi-Tamburini, G. Chiodelli, M. Arimondi, F. Maglia, G. Spinolo, Z.A. Munir, Electrical properties of Ni/YSZ cermets obtained through combustion synthesis, Solid State Ionics 110 (1998) 35–43.
[6] D. Skarmoutsos, A. Tsoga, A. Naoumidis, P Nikolopoulos, 5 mol% TiO_2-doped Ni-YSZ anode cermets for solid oxide fuel cells, Solid State Ionics 135 (2000) 439–444.
[7] R. O'Hayre, D.M. Barnett, F.B. Prinz, The triple phase boundary a mathematical model and experimental investigations for fuel cells, J. Electrochem. Soc. 152 (2005) A439–A444.
[8] H.C. Kim, I.J. Shon, J.E. Garay, Z.A. Munir, Consolidation and properties of binderless sub-micron tungsten carbide by field-activated sintering, Int. J. Refract. Met. Hard Mater. 22 (2004) 257–264.
[9] D.Y. Oh, H.C. Kim, J.K. Yoon, I.J. Shon, Simultaneous synthesis and consolidation process of ultra-fine WSi_2-SiC and its mechanical properties, J. Alloys Compd. 286 (2005) 270–275.
[10] H.C. Kim, D.Y. Oh, J. Guojian, I.J. Shon, Synthesis of WC and dense WC-5 vol.% Co hard materials by high-frequency induction heated combustion, Mater. Sci. Eng. A 368 (2004) 10–17.
[11] L.A. Chick, L.R. Pederson, G.D. Maupin, J.L. Bates, L.E. Thomas, G.J. Exarhos, Glycine–nitrate combustion synthesis of oxide ceramic powders, Mater. Lett. 10 (1990) 6–12.
[12] M. Chen, B.H. Kim, Q. Xu, B.K. Ahn, W.J. Kang, D.P. Huang, Synthesis and electrical properties of $Ce_{0.8}Sm_{0.2}O_{1.9}$ ceramics for IT-SOFC electrolytes by urea-combustion technique, Ceram. Int. 35 (2009) 1335–1343.
[13] K.S. Lee, S.W. Lee, J.H. Yu, D.W. Seo, S.K. Woo, Improvement of the stability of NiO-YSZ anode material for solid oxide fuel cell, J. Solid State Electrochem. 11 (2007) 1295–1301.
[14] F.L. Zhang, C.Y. Wang, M. Zhu, Nanostructured WC/Co composite powder prepared by high energy ball milling, Scripta Mater. 49 (2003) 1123–1128.
[15] N.Q. Minh, Ceramic fuel cells, J. Am. Ceram. Soc. 76 (1993) 563–588.